Romanian Reports in Physics, Vol. 68, No. 3, P. 1149–1158, 2016

STRUCTURAL CHARACTERIZATION AND OPTICAL PROPERTIES OF HYDROXYAPATITE/COLLAGEN MATRIX

CRISTINA LIANA POPA[1,2] M. ALBU[4], C. BARTHA[1], A. COSTESCU[5], C. LUCULESCU[6], R. TRUSCA[7], S. ANTOHE[2, 3, *]

[1] National Institute for Materials Physics, P.O. Box MG 07, Magurele, Romania
[2]University of Bucharest, Faculty of Physics, 405 Atomistilor Street, P.O. Box MG1, 077125, Magurele, Romania
[3]Academy of Romanian Scientists, Splaiul Independentei 54, 0505094, Bucharest, Romania
[4]Collagen Department, National Research & Development Institute for Textiles and Leather (INCDTP) – Division, Leather and Footwear Research Institute, Ion Minulescu Str. 93, 031215 Bucharest, Romania
[5]Hyperion University of Bucharest, 169 Calea Călăraşilor, 030615 Bucharest, Romania
[6]National Institute for Laser, Plasma and Radiation Physics, 409 Atomistilor St. P.O.Box MG 36, Bucharest, Magurele 077125 Romania
[7]S.C. METAV R&D S.A., 020011 Bucharest, Romania
*Corresponding author: santohe@solid.fizica.unibuc.ro

Received March 26, 2015

Abstract. This paper presents the synthesis and characterization of hydroxyapatite (HAp) and hydroxyapatite embedded in a collagen matrix (C-HAp6). The aim of this study was to investigate the influence of collagen on the structure and morphology of hydroxyapatite. According to the XRD patterns, the samples have the structure characteristic to hydroxyapatite. The FTIR and Raman spectra proved the successfully embedding of hydroxyapatite in the collagen matrix. Morphologically, the collagen increases the porosity of HAp. The collagen influences the structure and morphology of the hydroxyapatite causing a decrease of the mean particle size and/or a decrease of crystallinity while increasing the porosity.

Key words: hydroxyapatite, collagen, structure and morphology.

1. INTRODUCTION

With the development of modern medicine, the research field of tissue engineering has emerged due to the constant need for new and improved materials that could substitute human tissues and organs. Different diseases and injuries are the main causes that lead to surgeries that entail the replacement of the original tissue with an artificial one. In order for the surgery to be successful, the implanted material has to mimic as closely as possible the natural human tissue. The material must resemble the structural, mechanical and biological properties [1–2] of the replaced tissue. In the case of orthopedic and dental surgeries, the most commonly

used material for coatings is hydroxyapatite (HAp). Having the chemical formula $Ca_{10}(PO_4)_6(OH)_2$, hydroxyapatite is found in natural human hard tissue, being the main inorganic component of bone and teeth [3–5]. It has been proven that synthetic hydroxyapatite exhibits properties such as osteoconductivity and osteoinductivity which stimulate bone regeneration [6]. Because it is a biocompatible material, it has been widely used as a coating material for implanted devices [7–8]. Another important characteristic of HAp is its biodegradability. Previous studies [9–14] have shown that hydroxyapatite tends not to trigger a response from the immune system, embedding itself successfully in the surrounding tissue and degrading over time as the host tissue begins to regenerate.

On the other hand, considering that the human bone consists of an organic matrix formed of collagen reinforced with mineral hydroxyapatite, where the collagen represents 90% of its content [15], it is obvious why researchers have focused their attention on creating a new composite based on hydroxyapatite and collagen, in order to create a material that could mimic as much as possible the human hard tissue. Collagen is a biopolymer found in abundance in the structure of different human tissues like bones, cartilages and blood vessel walls [16]. The main properties that make collagen an interesting material are its ability to be resorbed by the human body and its ability to promote cell attachment [16]. In this context, previous studies [17–18] have proven that composites based on hydroxyapatite and collagens are biocompatible in humans and animals. One of the main objectives is to develop a material that can possess the properties of both hydroxyapatite and collagen in order to create a composite which could be considered as a candidate for clinical use.

The present study focuses on the synthesis and characterization of hydroxyapatite embedded in a collagen matrix, the aim being to emphasize the influence that collagen has on the structure and morphology of hydroxyapatite.

2. MATERIALS AND METHODS

2.1. SAMPLES

All the reagents used for the synthesis, including ammonium dihydrogen phosphate [$(NH_4)_2HPO_4$] and calcium nitrate [$Ca(NO_3)_2{\cdot}4H_2O$] were used as purchased, without further purification. Type I fibrillar collagen in gel form (Coll) with a concentration of 2.11% (w/w) was extracted from calf hide by acid and alkaline treatments as previously described [19]. Glutaraldehyde was purchased from Merck (Germany). Sodium hydroxide and phosphate buffer solution (PBS), pH = 7.4 were of analytical grade.

The $Ca_{10}(PO_4)_6(OH)_2$ ceramic powder was prepared maintaining the molar ration Ca:P = 1:67. $Ca(NO_3)_2{\cdot}4H_2O$ and $(NH_4)_2HPO_4$ were used as precursors in a co-precipitation synthesis method. Firstly, a predetermined amount of ammonium dihydrogen phosphate [$(NH_4)_2HPO_4$] was dissolved in deionized. Then, a designed

amount of calcium nitrate tetrahydrate was dissolved in deionized water. The two solutions have been mixed and the new obtained solution has been stirred constantly for 2 h by a mechanical stirrer at 100°C. The pH was constantly adjusted and kept at 10 during the reaction. Afterwards, the deposited mixtures were washed several times with deionized water and the final material (HAp) was dried at 100°C for 72 h in an electrical oven.

In order to obtain the sample containing hydroxyapatite embedded in a collagen matrix, 6 g of previously synthesized hydroxyapatite powder were added to 100 ml of a solution containing collagen. The resulted mixture was stirred continuously for 90 h and, finally, lyophilized using the Christ Model Delta 2–24 LSC freeze-dryer (Germany).

2.2. SAMPLE CHARACTERIZATION

X-Ray Diffraction (XRD). The XRD patterns have been obtained using a Bruker D8 Advance diffractometer, with a nickel-filtered Cu Kμ (λ = 1.5418 Å) radiation, and a high efficiency one-dimensional detector (Lynx Eye type) operated in integration mode. The patterns were collected in the 2θ range with a step of 0.02° and 34 s measuring time per step. The qualitative phase analysis was performed with the EVA software package and ICDD- PDF-2-database

Scanning Electron Microscopy (SEM). In order to investigate the structure and morphology of the samples, SEM studies have been performed using a HITACHI S2600N-type scanning electron microscope (SEM), operating at 25 kV in vacuum.

Fourier Transform Infrared Spectroscopy (FTIR). The functional groups present in the structure of the prepared samples were identified by FTIR spectroscopy using a Perkin Elmer, Spectrum BX spectrometer. The absorption spectra have been obtained using tablets containing with 99% KBr 1% of the studied nanopowder, the powder mixture being previously ground and pressed with a load of 10 tones. The spectra were recorded in the range of 400 to 4000 cm^{-1} with 4 cm^{-1} resolution.

Raman Spectroscopy. Complementary to FTIR studies, Raman spectra have been recorded with a FT Raman Bruker RFS 100 spectrophotometer which uses an excitation wavelength of 1064 nm. The laser power was set at 100 mW and the spectra were registered using up to 100 scans with a 4 cm^{-1} resolution.

Thermal Analysis. Differential thermal analysis (DTA) and thermal gravimetric analysis (TGA) were used in order to study the thermal behavior of the

prepared powders. For this purpose, a Shimatzu DTG-TA-50 and DTA 50 analyzer has been used in the 25–800 ^{o}C temperature range, air environment, and Al_2O_3 reference.

3. RESULTS AND DISCUSSIONS

In Fig. 1 are reported the diffractograms of the HAp (a) and C-HAp6 (b) samples. Both patterns show the characteristic peaks of hydroxyapatite, according to the International Center for Diffraction Data database, ICDD-PDF 9-0432. The XRD patterns indicate the presence of a majority phase corresponding to the hexagonal singony – $P_{63/m}$ space group associated to pure HAp.

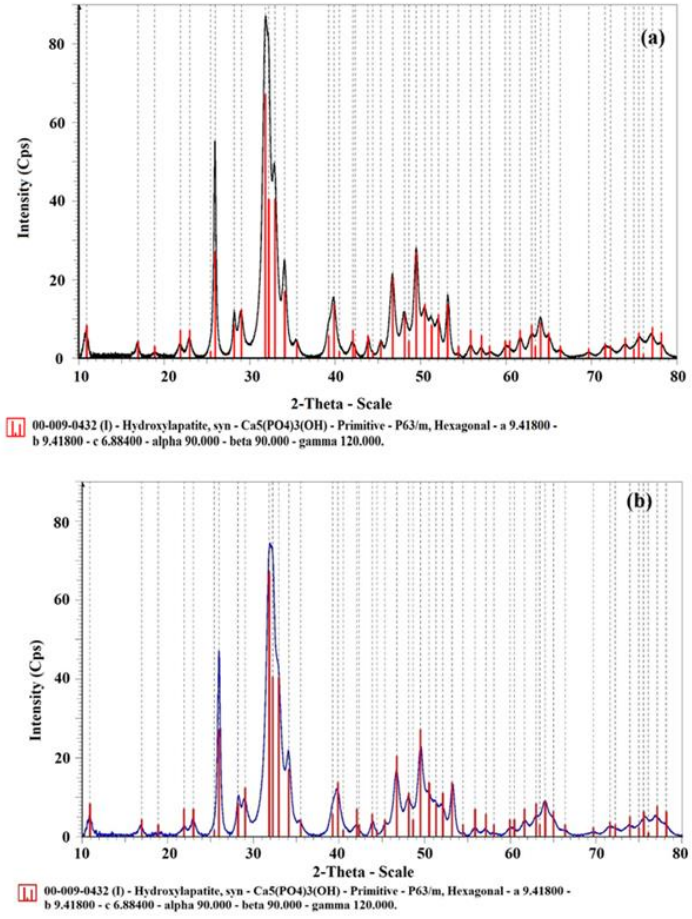

Fig. 1 – X-ray diffraction patterns of HAp (a) and C-HAp6 samples (b).

In addition, no other minority phase has been detected. On the other hand, a slight decrease of the peaks intensity could be observed in the case of C-HAp6. This behavior could be caused to a decrease of the degree of crystallinity.

The morphology of the HAp and C-HAp6 powders was investigated by scanning electron microscopy (SEM). The results are presented in Fig. 2a–b. The HAp nanoparticles exhibit an acicular morphology. Moreover, the particles tend to agglomerate due to their small dimensions. On the other hand, the C-HAp6 nanoparticles exhibit an increase of the porosity. This behavior is probably due to the presence of the collagen matrix.

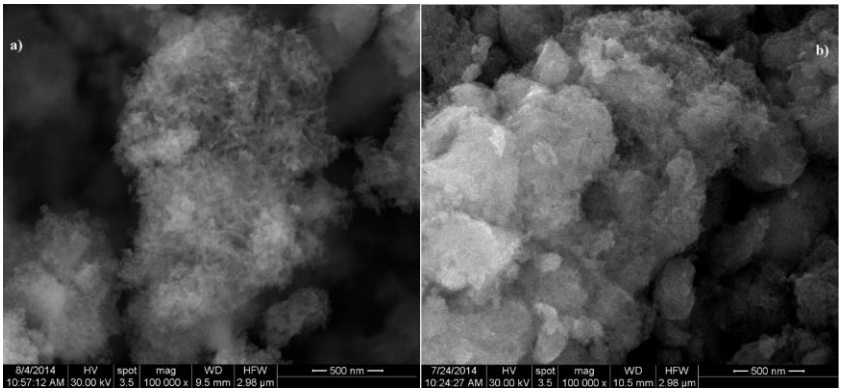

Fig. 2 – SEM images of HAp (a) and C-HAp6 samples (b).

The results obtained by SEM an XRD studies conduct to the same conclusion: the presence of the collagen matrix leads to a decrease of the mean particle size and/or a decrease of the cristalinity.

The chemical changes of the HAp and C-HAp6 samples were investigated by thermal studies. The thermogravimetric analysis (TGA) and the differential thermal analysis (DTA) curves of the HAp and C-HAp6 samples are shown in Fig. 3 and Fig. 4 respectively. From the DTA curve analysis the temperature of the maximum process speed was determined (exothermic peaks). In the DTA curve of HAp sample (Fig. 3) two peaks can be observed. The first peak is at 161 ^{o}C and the second, very wide maximum appears at around 700 ^{o}C. On the other hand, in the DTA curve of C-HAp6 sample three peaks can be observed (Fig. 4). The first peak is wide and appears at 161 ^{o}C. In the DTA curve of C-HAp6 sample, the second peak appears at 330 ^{o}C and the third, very wide peak appears at around 730 ^{o}C. For both samples, the first weight loss occurs for temperatures up to 161 ^{o}C (sample HAp) and up to around 331 ^{o}C (sample C-HAp6) respectively. This loss may be assigned to the water molecules that are physically adsorbed on the samples and are weakly bound [20–21]. The first weight loss for the HAp samples is 2.46 %

while for the C-HAp6 sample the first weight loss is around 6%. The second loss of mass occurs after 620 ^{o}C (2.57%) for the HAp sample and corresponds to the total loss of mass. In the case of C-HAp6, a major weight loss occurs between 330–620 ^{o}C (17.60%).

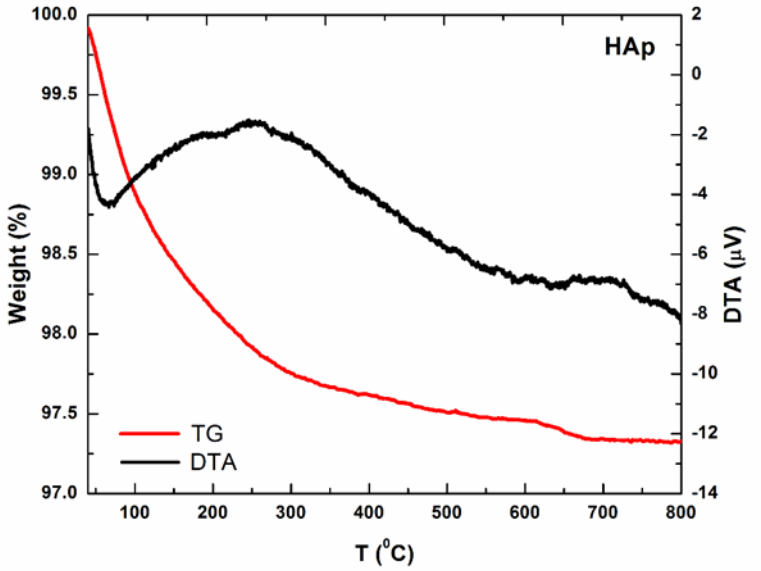

Fig. 3 – TGA and DTA curves of the HAp sample.

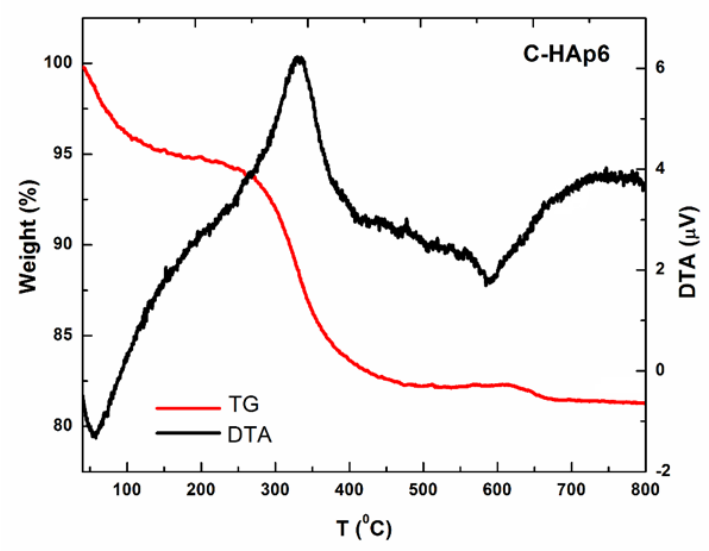

Fig. 4 – TGA and DTA curves of the C-HAp6 sample.

For both samples the weight loss remains constant after 620 °C. The weight loss that occurs around 620 °C is approximately 0.12 % for the HAp sample (Fig. 3) and approximately 0.80% for the C-HAp6 sample. The second weight loss (17.60 %) observed in the C-HAp6 sample (Fig. 4), between 300–620 °C, can be attributed to the release of water related to collagen and to the release of small molecular products produced by the thermal degradation of collagen. According to previous studies conducted by Tegza *et al.* [22] the second mass loss may be caused by thermal and oxidative destruction processes characterized by a more rapid decomposition.

The functional groups present in the prepared samples were investigated by aid of FT-IR studies (Fig. 5). The spectra registered for the hydroxyapatite and hydroxyapatite with collagen showed the apatite characteristic bands. The presence of phosphate group PO_4^{3-} is highlighted by the 472 cm^{-1} band associated to the ν_2 double degenerated bending mode [23–26] and the bands found at 568 and 600 cm^{-1} characteristic to the ν_4 vibration mode [27–30].

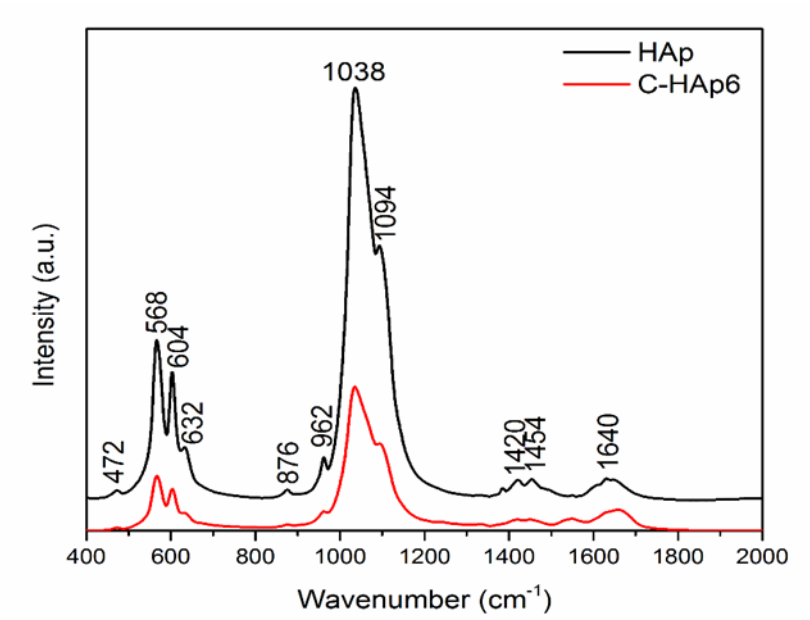

Fig. 5 – FT-IR spectra of HAp (a) and C-HAp6 samples (b).

Furthermore, the band registered at 962 cm^{-1} is evidence of the ν_1 nondegenerated symmetric stretching mode of the P-O bond [23–25, 31–32] and the bands found at 1036 and 1095 cm^{-1} are associated to the ν_3 vibration mode of the PO_4^{3-} functional group [27–29]. On the other hand, the CO_3^{2-} functional group

is highlighted by the presence of several vibration bands. At around 870 cm^{-1} can be found the band characteristic to the ν_2 vibration mode [27–28, 30] and the stretching vibrations of the CO_3^{2-} group are highlighted by the 1415 and 1450 cm^{-1} bands [23–28, 33]. The band present at 1550 cm^{-1} is also proof of the presence of CO_3^{2-} functional group in the studied samples. The hydroxyl group from the structure of the samples is emphasized by the 631 cm^{-1} band [34]. Moreover, the bands present in the region 1600–1700 cm^{-1} are characteristic to the H-O-H bonds of water lattice. In the case of the spectrum registered for the C-HAp6 sample, it can be clearly observed that in the 1600–1700 cm^{-1} region, the band is wider. This behavior can be explained by an overlapping of the water lattice band and the band associated to C=O stretching mode of the amide I present in the FT-IR spectrum of collagen [35]. Also, in the spectrum of hydroxyapatite with collagen, at 1548 cm^{-1} can be observed a vibrational band associated to Amide II [36]. Comparing the two spectra it can easily be observed that the influence of collagen causes a decrease of the peak intensities and a general widening of all the bands.

Complementary to FTIR studies, Raman Spectroscopy measurements have been registered. In Fig. 6 are evidenced the two spectra of hydroxyapatite and hydroxyapatite embedded in a collagen matrix samples. It can easily be observed that the two spectra follow the hydroxyapatite characteristic spectrum.

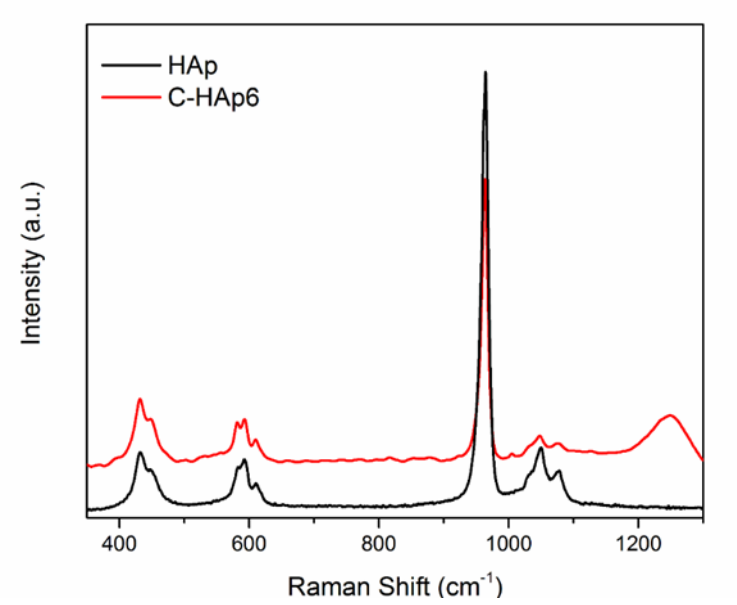

Fig. 6 – Raman spectra of HAp (a) and C-HAp6 samples (b).

Therefore, through Raman studies have been revealed the bands characteristic to PO_4 functional group. The asymmetric and symmetric stretching

modes of the PO_4 group are highlighted by the bands found at around 1076 cm^{-1}, 1046 cm^{-1}, 1030 cm^{-1} and 961 cm^{-1} respectively [29, 35, 23]. On the other hand, the triply degenerated bending mode of the O-P-O bond is evidenced by the bands located around 610 cm^{-1}, 594 cm^{-1} and 582 cm^{-1} [29, 35, 23] while the doubly degenerated bending mode determines the presence of 433 and 447 cm^{-1} bands [23]. An additional band can be noticed in the spectrum of the sample containing collagen at around 1254 cm^{-1} characteristic to Amide III [37]. Like in the case of FTIR spectra, the influence of the collagen determines a decrease of the peak intensities as well as a widening and a smoothing of all the peaks.

4. CONCLUSIONS

The results of this study emphasize the influence of embedding hydroxyapatite in a collagen matrix. For this purpose, the structure, morphology and chemical changes of the prepared samples have been studied. The XRD patterns suggest that both samples have the hydroxyapatite characteristic structure, although the collagen seems to induce a decrease of the crystallinity. The decrease of the sample crystallinity has also been observed in the SEM images. A decrease of the mean particle size and an increase of the porosity could also be observed in the SEM images. Regarding the functional groups present in the obtained samples, the FTIR and Raman spectra suggest the presence of HAp characteristic bands associated mainly to phosphate, carbonate and hydroxyl groups, the addition of collagen inducing a decrease of the peak intensities as well as a widening and a smoothing of all the peaks. Thermal studies have been also performed in order to determine the chemical changes of the HAp and C-HAp6 samples. Analyzing the DTA curves, the exothermic peaks have been highlighted. HAp has two peaks at 161 ^oC and 700 ^oC while for the C-HAp sample three peaks are observed at 161 ^oC, 330 ^oC and 730 ^oC respectively. Also, the major weight loss for both samples occurs before 620 ^oC, for higher temperatures the weight loss remaining constant.

In conclusion, this study showed that embedding synthetic hydroxyapatite in a collagen matrix leads to the formation of a new compound with a HAp characteristic structure, with a smaller mean particle size than pure HAp, which exhibits a higher porosity and a lower crystallinity.

Acknowledgements. We specifically thank Dr. Daniela Predoi for the interpretation of TGA, DTA experimental data and for all the support and guidance provided throughout the entire process of writing this manuscript. We acknowledge Dr. Ciobanu Carmen for technical assistance in XRD interpretation and for the support of the manuscript. This work was supported by the PN II 259/2014 project and PN II 221/2014 project. Also, this work was supported by the strategic grant POSDRU/159/1.5/S/137750, "Project Doctoral and Postdoctoral programs support for increased competitiveness in Exact Sciences research" cofinanced by the European Social Found within the Sectorial Operational Program Human Resources Development 2007–2013.

REFERENCES

1. A. Chandrasekar, S. Sagadevan and A. Dakshnamoorthy, Int. J. Phys. Sci. **8**, 1639–1645 (2013).
2. S. Yang, K.F. Leong, Z. Du and C.K. Chua, Tissue. Eng. **7**, 679–689 (2001).
3. E. Fujii, M. Ohkubo, K. Tsuru, S. Hayakawa, A. Osaka, K. Kawabata, C. Bonhomme and F. Babonneau, Acta. Biomater. **2**, 69–74 (2006).
4. D.A. Puleo, L.A. Holleran, R.H. Doremus and R. Bizios, J. Biomed. Mater. Res. **25**, 711–723 (1991).
5. R. Garcia and R.H. Doremus, J. Mater. Sci. Mater. Med. **3**, 154 – 156 (1992).
6. K.J.L.Burg, S. Porter and J.F. Kellam, Biomaterials. **21**, 2347 – 2359 (2000).
7. Y.J. Wang, J.D. Chen, K. Wei, S.H. Zhang and X.D. Wang, Mater. Lett. **60** 3227–3231 (2006).
8. C.S. Ciobanu, S.L. Iconaru, P. Le Coustumer, L.V. Constantin and D. Predoi, Nanoscale. Res. Lett. **7**, 324–332 (2012).
9. G. Krishnamurithy, M. Raman Murali, M. Hamdi, A.A. Abbas, H.B. Raghavendran and T. Kamarul, Ceram. Int. **40**, 771–777 (2014).
10. H. Yoshikawa, N. Tamai, T. Murase and A. Myoui, J. R. Soc. Interface. **6**, S341–S348 (2009).
11. C.S. Ciobanu, F. Massuyeau, L.V. Constantin and D. Predoi, Nanoscale. Res. Lett. **6**, 613–620 (2011).
12. C.S. Ciobanu, C.L. Popa and D. Predoi, J. Nanomater. **2014**, 1–9 (2014).
13. C.S. Ciobanu, E. Andronescu and D. Predoi, Dig. J. Nanomater. Bios. **6**, 1239–1244 (2011).
14. D.Predoi and R.A. Vatasescu-Balcan, J. Optoelectron. Adv. M. **10**, 152–157 (2008).
15. E. Sachlos, D.A. Wahl, J.T. Triffitt and J.T. Czernuszka, Acta. Biomater. **4**, 1322–1331 (2008).
16. D.A. Wahl and J.T. Czernuszka, Eur. Cells. Mater. **11**, 43–56 (2006).
17. C.M. Serre, M. Papillard, P. Chavassieux and G. Boivin, Biomaterials. **14**, 97–106 (1993).
18. A. Scabbia and L. Trombelli, J. Clin. Periodontol. **31**, 348–355 (2004).
19. M.G. Albu, *Collagen Gels and Matrices for Biomedical Applications*, Lambert Academic Publishing, Saarbrücken, 2011.
20. D. Predoi, Dig. J. Nanomater. Bios. **2**, 169–173 (2007).
21. D. Predoi, Dig. J. Nanomater. Bios. **5**, 373–377 (2010).
22. M. Tegza, O. Andreyeva and L. Maistrenko, Chemine Technologija **59**, 40–45 (2012).
23. S. Koutsopoulos, J. Biomed. Mater. Res. **62**, 194–207 (1974).
24. B.O. Fowler, Inorg. Chem. **13**, 194–207 (1974).
25. C.S. Ciobanu, E. Andronescu, B.S. Vasile, C.M. Valsangiacom, R.V. Ghita and D. Predoi, Optoelectron. Adv. Mat. **4**, 1515–1519 (2010).
26. W.E. Klee and G. Engel, J. Inorg. Nucl. Chem. **32**, 1837–1843 (1970)
27. A. Slosarczyk, Z. Paszkiewicz and C. Paluszkiewicz, J. Mol. Struct. **744**–**747**, 657–661 (2005).
28. C.L. Popa, C.S. Ciobanu, S.L. Iconaru, M. Stan, A. Dinischiotu, C.C. Negrila, M. Motelica-Heino, R. Guegan and D. Predoi, Cent. Eur. J. Chem. **12**, 1032–1046 (2014).
29. C.S. Ciobanu, F. Massuyeau, E. Andronescu, M.S. Stan, A. Dinischiotu and D. Predoi, Dig. J. Nanomater. Bios. **6**, 1639–1647 (2011).
30. R.M. Wilson, J.C. Elliott, S.E.P. Dowker, L.M. Rodriquez-Lorenzo, Biomaterials **26**, 1317–1327 (2005).
31. S.J. Gadaleta, E.P. Paschalis, N.P. Camacho, F. Betts, R. Mendelhson and A.L. Boskey, *Fourier Transform Infrared Spectroscopy of Synthetic and Biological Apatites*, Plenum Press, New York, 1995, pp. 283–294.
32. C.B. Baddiel and E.E. Berry, Spectrochim. Acta. A **22**, 1407–1416 (1966).
33. S. Raynaud, E. Champion and D. Bernache-Assollant, Biomaterials **23**, 1065–1072 (2002).
34. C.S. Ciobanu, S.L. Iconaru, F. Massuyeau, L.V. Constantin, A. Costescu and D. Predoi, J. Nanomater. **2012**, 1–9 (2012).
35. M.C. Chang and J. Tanaka, Biomaterials **23**, 4811–4818 (2002).
36. M.M. Figueiredo, J.A.F. Gamelas and A.G. Martins, *Infrared Spectroscopy – Life and Biomedical Sciences*, InTech, 2012.
37. K. Kalonakis, M. Orkoula and C. Kontoyannis, Nemertes, 2012.